Available online at www.sciencedirect.com
ScienceDirect
Thermochimica Acta 454 (2007) 116–127
thermochimica acta
www.elsevier.com/locate/tca

Thermal decomposition of 4-amino-1,2,4-triazolium nitrate under infrared laser heating

Jianquan Li, Thomas A. Litzinger*

Department of Mechanical and Nuclear Engineering, The Pennsylvania State University, University Park, PA 16802, USA

Received 2 June 2006; received in revised form 29 November 2006; accepted 7 January 2007
Available online 19 January 2007

Abstract

The objective of this work is to study the behavior of an ionic liquid, 1-H-4-amino-1,2,4-triazolium nitrate, during thermal decomposition driven by an infrared laser (10.6 μm). The focus was to understand the initial decomposition reactions and subsequent reactions that lead to ring decomposition and eventually to ignition. A triple quadrupole mass spectrometer with molecular beam sampling was used to obtain gaseous decomposition species of the sample. The principal mass peaks that may contain multiple masses were analyzed through tandem mass techniques. The experiments were conducted at a laser heat flux of 100 W/cm^2 in helium at 1 atm. To assist in interpreting the data, three other materials were also tested, 4-amino-1,2,4-triazolium hydrochloride, 4-amino-1,2,4-triazole, and 1-H-1,2,4-triazole. The results show that the most probable route to initiate the decomposition of the 1-H-4-amino-1,2,4-triazolium nitrate is through proton transfer from N_1 site to the nitrate forming a neutral pair, nitric acid and amino-triazole. Subsequent reactions involve decomposition of the neutral pair and their interactions.

Keywords: Ionic liquid; 4-Amino-1,2,4-triazolium nitrate; Thermal decomposition; Mass spectrometry

1. Introduction

Room temperature ionic liquids are of growing importance and interest due to their potential as environmentally friendly solvents, electrolytes, lubricants, and heat transfer media [1–7]. The growth in importance can be traced largely to the significant finding that *N*,*N*′-dialkylimidazolium and *N*-alkylpyridinium salts of common weakly coordinating anions (such as $AlCl_4^-$, BF_4^-, $CF_3SO_3^-$) are liquids at or near room temperature [8,9]. Salts that have a melting point below ca. 100 °C are defined as ionic liquids. The phase diagram for 1-ethyl-3-methylimidazolium chloride-aluminum(III) chloride, [emim]Cl-$AlCl_3$, shows that melting temperatures below −90 °C are possible [10]. Absence of strong hydrogen bonding in these ionic liquids is regarded as contributing to the low melting points [11]. Other important aspects include asymmetry of the cation, delocalization of the cation charge, addition of solvent-like tails, and nonalignment of ion pairs [12,13]. Properties of ionic liquids include negligible vapor pressure, high electrical conductivity, wide electro-chemical window, tolerance to strong acids, and excellent thermal and chemical stability [11]. Ionic liquids typically consist of nitrogen containing cations and inorganic anions. In addition to the previously mentioned *N*-alkylpyridinium and *N*,*N*′-dialkylimidazolium, common building blocks of ionic liquids include the alkylammonium and alkylphosphonium cations as well as water-insoluble $[PF_6]^-$ and water-soluble $[CH_3CO_2]^-$, $[CF_3CO_2]^-$, Br^-, Cl^-, I^-, $[Al_2Cl_7]^-$ and $[NO_3]^-$ anions.

Recently, these materials have garnered interest in the combustion community because of their unique properties including negligible vapor pressure, high density, and high solubility in many polar solvents. Potential applications include systems where low toxicity and high stability are of great importance such as gas generation for air bags. Materials of interests include substituted heterocyclic cations such as those mentioned above, paired with highly oxygenated anions such as nitrate, perchlorate, and dinitramide, to achieve appropriate stoichiometry for the application of interest. Additional cations of particular interest from an ignition and combustion point of view include triazolium and tertrazolium.

* Corresponding author at: 201B Hammond Building, The Pennsylvania State University, University Park, PA 16802, USA. Tel.: +1 814 865 4015; fax: +1 814 865 4021.
E-mail address: TAL2@psu.edu (T.A. Litzinger).

0040-6031/$ – see front matter © 2007 Elsevier B.V. All rights reserved.
doi:10.1016/j.tca.2007.01.013

A large number of studies are available in the literature that involve compounds based on the heterocyclic triazole ring structure. Such studies have in large part been driven by the need to find an explosive with similar performance characteristics to RDX and HMX, but with much reduced sensitivity to external stimuli such as slow cook-off, impact, and electrostatic discharge. As a result of synthesis efforts, 5-nitro-2,4-dihydro-3*H*-1,2,4-triazole-3-one (NTO) was developed in the early 1980s, and since has been the focus of numerous thermal decomposition studies [14–31]. Furthermore, metallized salts based on the triazole has also been synthesized as catalysts and their thermal decomposition behavior examined by various diagnostic techniques [32–40], as well as amine [14] and arylamonium [41,42] salts of NTO. A study of the thermal rearrangement of fused diaryl-v-trialoium salts to neutral indazole derivates is available [43]. Additionally, novel triazolium anions have been synthesized and discussed [44]. However, information on decomposition of triazolium cation appears to be limited. In particular, little experimental data on the condensed-phase processes leading to ignition and combustion of triazolium salts has appeared in the literature.

This paper reports a recent experimental effort with an objective of identifying the initiation and secondary reactions in the condensed phase that lead to ignition and combustion. An additional objective was to provide data for researchers performing molecular dynamics simulations of ionic liquids as well as researchers synthesizing these compounds. In the work reported in this paper, a model ionic liquid, 1-H-4-amino-1,2,4-triazolium nitrate, was selected for testing. The material was synthesized at Edwards AFB. The compound was studied using mass spectrometric methods during IR laser-driven decomposition.

2. Experimental

The experimental setup is schematically shown in Fig. 1. The main facilities include a heating source, a windowed test chamber, a sample holder, as well as a triple quadrupole molecular beam mass spectrometer (TQ-MBMS).

2.1. Test chamber

A small test chamber is used to minimize the distance from the sample to the sampling orifice. The chamber is marked in the figure by a circle to show the chamber size relative to the mass spectrometer. To reveal the details of the chamber, an enlarged sketch is presented in the figure to show the chamber cross-section. The test chamber is made of stainless steel. The body of the chamber is a 7.0 cm circular disk with a thickness of 2.0 cm. One side of the chamber interfaces with the sampling unit of the TQ-MBMS through a specially designed flange, and the other connects to a background gas source (argon or helium). A sample holder, also made of stainless steel, brings a sample through a stepped hole on the bottom of the chamber up to a point that is 1.5 mm below the centerline of the sampling orifice and 10 mm from the orifice. The sample is confined in a recessed cup (1.25 mm in diameter and 1.5 mm in depth) on the top of the sample holder.

The energy source for heating the samples is a high-power CO_2 laser with a maximum power output of 800 W in continuous wave mode. After passing through a collimating aperture (5 mm), the laser beam enters the test chamber along a narrow passage and then through a potassium chloride (KCl) window, which is 97% transmissive to the 10.6 μm laser beam. The beam size in the test chamber is determined by the passage diameter of 2.5 mm, which is selected to be twice that of the sample surface so that a largely uniform beam profile is achieved over the sample surface.

An inert gas (helium or argon) is introduced into the test chamber as a background as well as a carrier for the decomposition products. A standard gas handling system (a regulator and three valves) controls the gas flow rate.

2.2. Triple quadrupole mass spectrometer

The sampling and analysis of gaseous species were performed using a triple quadrupole molecular beam mass spectrometer; the method is described in further detail elsewhere [45,46]. As shown in Fig. 1, the sampling orifice (100 μm) is fabricated on a disc plate (12 mm in diameter and 1.5 mm in thickness), which was purchased from Lenox Laser. A skimmer, placed 10 mm behind the disc orifice, has an aperture of 1.5 mm and a length of 50 mm with 55°/60° interior/exterior angles. The skimmer was obtained from Beam Dynamics, Inc. The disc-skimmer distance is adjustable by using spacers for better beam performance.

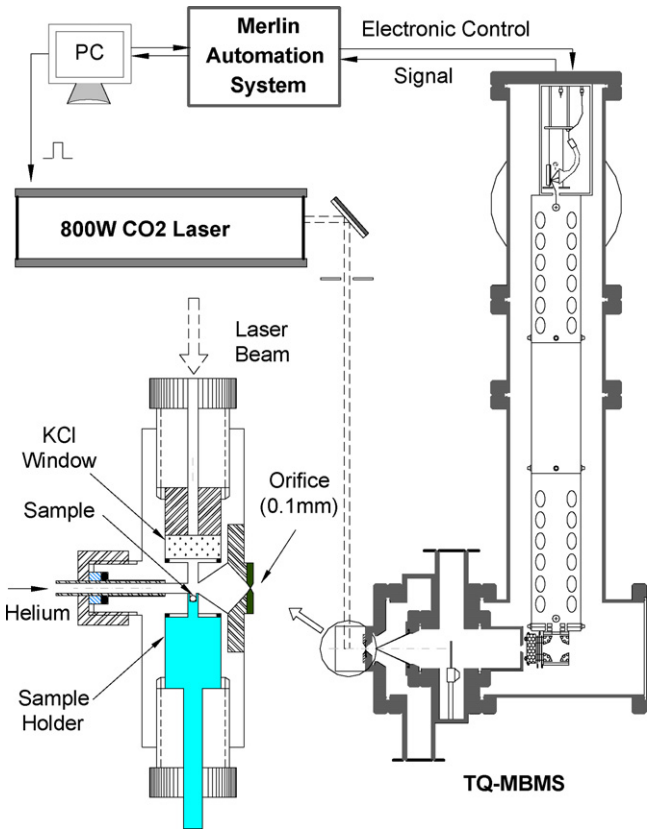

Fig. 1. Schematic of experimental setup.

The sample gases are drawn through the orifice and into the mass spectrometer by two diffusion pumps and two turbomolecular pumps as well as their backing pumps forming a three-stage differential vacuum system ($10^{-3}/10^{-5}/10^{-7}$ torr) to meet the requirement imposed by the orifices. Ions are produced during electron impact (EI) in the ion region of an Extrel cross-beam-deflector ionizer, which is a combination of an axial ionizer mounted perpendicularly to the mass filter axis and a small quadrupole deflector energy filter. The energy-filtering capability of this ionizer provides great improvement in its sensitivity, because tuning the lenses of the energy filter can add energies up to hundreds of electron volts (eV) to the deflected beam. The right-angle configuration dramatically increases signal-to-noise by removing unwanted components of the sample, such as photons, neutrals and even particulates, since they are directly pumped away by the turbo pump behind the ionizer. This configuration also helps to reduce contamination of the quadrupoles and the detector for better performance in corrosive and high-particulate applications.

Two modes can be selected for the mass filtering operation of mass spectrometer: "parent" mode and "daughter" mode. Using the daughter mode of operation, it is possible to identify and differentiate N_2, CO, C_2H_4 at m/z 28, NO, CH_2O at m/z 30, and N_2O, CO_2 at m/z 44. In the daughter mode, the ion of interest, often referred to as the "parent", is selected in the first quadrupole (Q1). The parent ions then enter the second quadrupole (Q2) and are fragmented into smaller species, the daughters, by the process of collision-induced dissociation (CID) with an inert gas separately supplied into Q2. Argon was used as the collision gas in this study to minimize its contributions to fragmented species. The daughters, at masses less than their parent, are detected in the third quadrupole (Q3). For complex parent ions, some of the daughters might overlap if the parents contain common structures. In the present study, however, at least one unique daughter could be acquired for each parent.

Detection of the ions that pass through the mass filters is performed using a channeltron multiplier with a conversion dynode. An Extrel Merlin Automation system provides full electronic control of the TQMS system and performs data acquisition and reduction.

Several methods of calibration are used to obtain the sensitivity coefficients (intensity/concentration) of each species. The most stable species are calibrated directly with the gas mixtures of known concentration. To calibrate water, water vapor is acquired from liquid water that was vaporized by the CO_2 laser. Typically, the sensitivity factors are repeatable within 10%. The calibration factor of species for which standards are not readily available, e.g., HCN, is estimated by correlating the signal intensity to that of calibrated species with a similar appearance potential through the ratio of their ionization cross sections [47].

For all the calibrations and in the actual tests, ionization energy of 22 eV is used to minimize fragmentation of molecules and still get a sufficient number of ions to produce acceptable intensities. However, this setting is still high compared to the ionization energies of 9–15 eV for most organic compounds, thus, some fragments are formed and contributed to the signals at masses other than the parent mass. In such instances, these signals are subtracted from the mass signal of interest. For quantitative analysis, species information will be reported as normalized mole fractions by totaling the measured concentrations of the sampled species and dividing each concentration by this total. The normalization eliminates the effect of sample temperature on the observed signal intensities since the temperature dependence cancels out. This method also cancels out the effect of probe orifice blockage on signal intensity. To check if there are any major species missing during the sampling, element balances are performed using the measured more fractions.

2.3. Sample

The material of major interest in this work is 1-*H*-4-amino-1,2,4-triazolium nitrate (4-ATAN). To assist in interpreting the results, experiments were also performed with 4-amino-1,2,4-triazole hydrochloride (4-ATACl), 4-amino-1,2,4-triazole (4-ATA), and 1-*H*-1,2,4-triazole (*h*TA). The molecular structures of these materials are shown in Fig. 2. Under standard conditions, these materials are all solids, with the chloride salt being yellow-greenish and the other three being white in color. The melting points are 69 °C (4-ATAN), 86–89 °C (4-ATACl), 84–86 °C (4-ATA), and 120–121 °C (*h*TA). The nitrate salt was synthesized by AFB at Edwards; others were purchased from Sigma–Aldrich Company. The sample size used in each test was about 0.5 mg.

Initial tests were run in a larger (16.5 cm × 16.5 cm × 25.4 cm) windowed test chamber [48] so that the event could be video-taped for observation of the behavior of a sample duing laser heating at varying heat fluxes. The video was acquired using a Sony camcorder. In addition, a Pulnix video CCD camera equipped with a Nikon macro lens in conjunction with a TV screen was used to provide real-time monitoring of the event. In

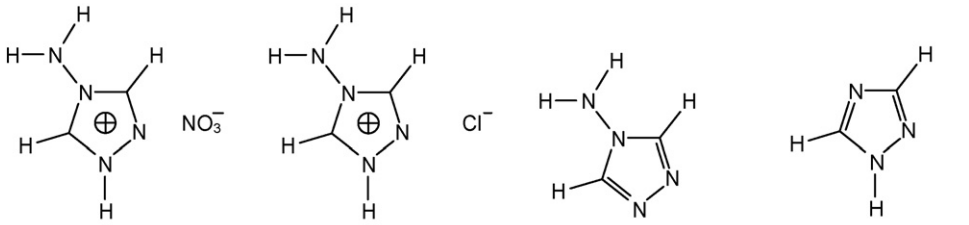

Fig. 2. Molecular structures of 4-ATAN, 4-ATACl, 4-ATA, and *h*TA.

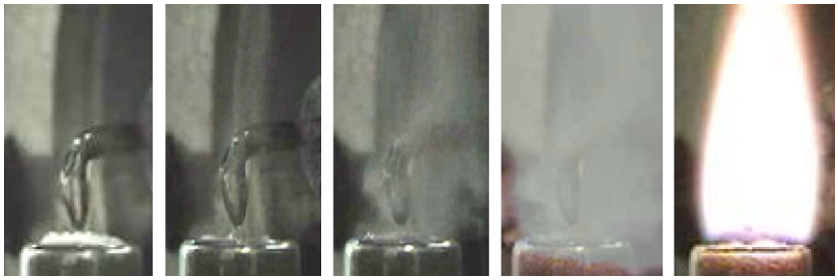

Fig. 3. Laser-driven vaporization and burning of 4-ATAN at 200 W/cm^2 in 1 atm. air.

the initial tests, a larger quantity of sample (∼5 mg) was placed on a quartz sample holder, and an angled microprobe (see Fig. 3) was used to monitor the species evolution.

3. Results and discussion

3.1. Ignition and burning of 4-ATAN

In atmospheric air conditions, 4-ATAN starts to melt and vaporize at a laser heat flux about 35 W/cm^2; ignition of the sample is not achived until the heat flux reaches 150 W/cm^2. At this condition, an ∼4 s delay occurs between the trigger of the laser and the appearance of a visible flame, during which "smoking" is observed. In an inert environment, e.g., helium, ignition occurs at a higher heat flux around 200 W/cm^2. Fig. 3 presents a few images showing the "smoke" and flame at a heat flux of 200 W/cm^2 in 1 atm. air. It shows that prior to the appearance of a luminous flame (5th image), the solid sample (1st image) melts (2nd image) and vaporizes (3rd and 4th images) into gaseous species. Bubbles were observed to develop during melting. The onset of ignition is about 3.2 s after triggering the laser.

A few tests were run to get a species profile through the smoking region starting from the sample surface up to 6 mm above the sample surface. The profile reveals consistency in species detected across this region, an indicator that early decomposition ocurrs in the condensed phase. However, Dessiaterik et al. [49], who used IR lasers to ablate imidazolium salts, suggested decomposition would occur in the gas phase, since the laser heating usually produces high heating rates, with which vaporization rate is higher than decomposition rate. Considering the fact that their laser ablation tests were conducted under a vaccum condition, it is possible that decomposition occurs in the gas phase. Also, triazoles have a higher melting point and higher enthalpies of phase transitions, which would reduce the vaporization rate versus the decomposition rate. In addition, the beam size and pulse width of the lasers used are different, both of which would cause the difference observed in the two studies.

3.2. Measurement of species

Species measurement using the quartz microprobe provides greater flexibility in choosing the sampling point relative to the sample surface, but loss of species due to condensation along the inner wall of the narrow probe (∼2 mm of i.d. and 70 mm in length) proved to be a major problem. For example, species at m/z 69 and 84 were missing in initial attempts to detect products from 4-ATAN using the microprobe. However, these species were seen in additional tests with molecular beam sampling. Therefore, the configuration of an orifice in a thin disc coupled with a cone-shaped skimmer was used for all the species data presented in the paper.

To help eliminate m/z interference from N_2 and O_2 present in an air background, helium was used as the carrier gas. Obviously, minimizing the heating power would help to identify initial steps leading to decomposition, but a compromise had to be made to obtain a better signal intensity. Preliminary tests were conducted to select a proper laser heat flux level by keeping in mind that minimum heat flux would be used as long as an acceptable signal intensity is achieved for each material studied. As mentioned above, the 4-ATAN material starts to vaporize at about 35 W/cm^2, at which, however, the mass signals are very weak, and even at 50–75 W/cm^2, the signal is still not good. Therefore, an even higher heat flux at 100 W/cm^2 was used throughout the tests with 4-ATAN in helium. No ignition was achieved at this heat flux.

Fig. 4 presents a typical mass spectrum of 4-ATAN taken at the moment when the number of total ion counts reached a maximum. The background has been subtracted from the spectrum. To cover all possible decomposition products, the scan was made over a range of mass-to-charge ratio (m/z) from 1 to 150 amu (147 for the 4-ATAN molecule). The consistently detected species were distributed within a range of m/z 14–84, as shown in the figure. No species at m/z higher than 84 were observed.

Species temporal evolution during decomposition is shown in Fig. 5, where temporal profiles of all the detected masses are presented in three plots to improve clarity. It should be noted that

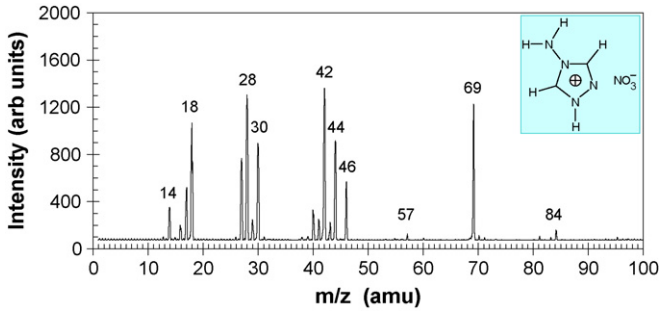

Fig. 4. A typical mass spectrum of 4-ATAN during decompostion driven by CO_2 laser heating at 100 W/cm^2 in an 1 atm. helium evironment.

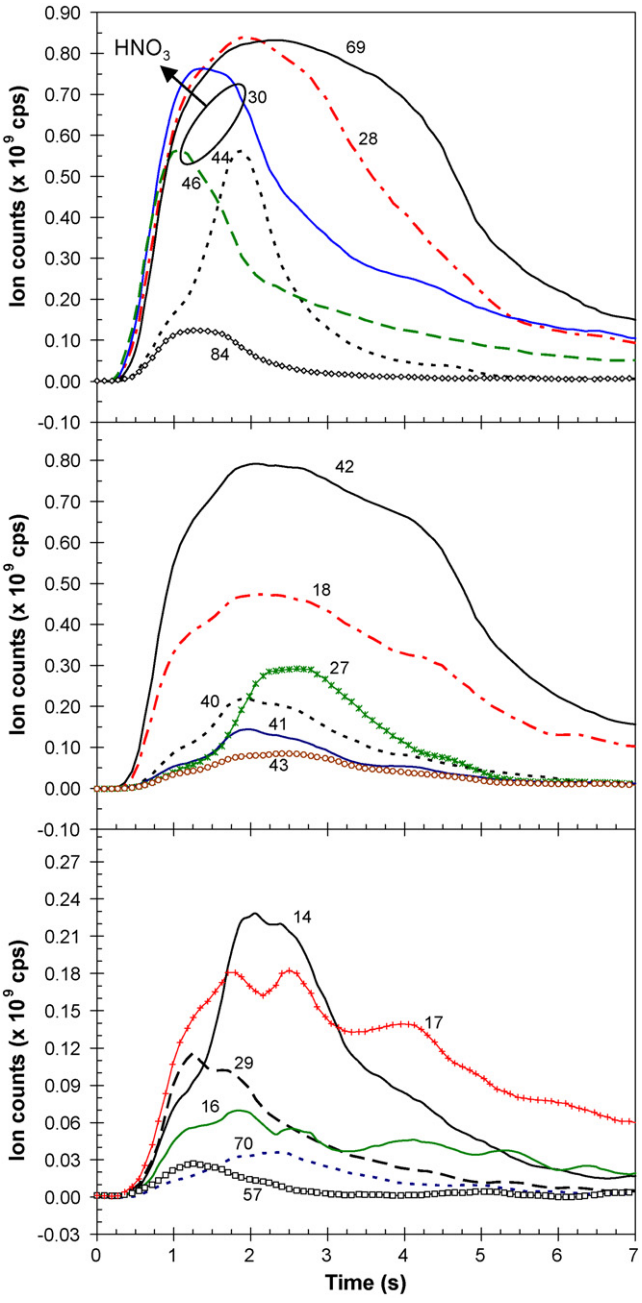

Fig. 5. Temporal evolution of decompostion products of 4-ATAN at 100 W/cm^2.

slight variation from test to test does exist, but the general trend in the temporal evolution of these species is the same. The plots in Fig. 5 reveal that the decomposition proceeds in several steps: some species are formed mainly in early steps, for example, *m*/*z* at 30, 44, 46, and 84; some are seen mainly in later steps, such as *m*/*z* at 27, 40, 41, and 43, while other species like *m*/*z* 69, 42, 28, 18, and 17 are observed in a wider range of time. The time sequence in the appearance of different species indicates that the cation ring remains intact for some time and then opens in later decomposition.

Assignment of each *m*/*z* value to a particular species is straightforward in some casess, for instance, *m*/*z* at 18 representing H_2O. However, additional experiments with daughter mode operation are needed in order to identify and differentiate species that have the same *m*/*z* value, such as N_2O and CO_2, both having *m*/*z* at 44.

3.3. Identification and differentiation of species

Another series of experiments were performed with the TQ-MBMS operating in daughter mode for MS/MS analysis, and the results are summarized in Table 1. In the table, both the parent ions and daughter ions are listed in a decending order of intensity, and a dash "–" indicates that daughter mode tests were not performed for that parent species. Most of the parent ions were identified through analysis of their corresponding daughter ions by comparison with standard daughters from calibration tests. Some parent species were identified by comparing the results of 4-ATAN with that of 4-ATA and/or *h*TA. A few assignments remain tentative due to the lack of standard daughter spectra or comparison data.

The electron energy supplied to the ionizer was relatively low (22 eV), so the chance of producing doubly charged species is small. Therefore, the mass to charge ratio of each ion is assumed to equal the molecular weight of the corresponding molecule. Based on this assumption, *m*/*z* 28 is considered to have two candidates for the parent species, namely N_2 and CO. However, the lack of daughter at *m*/*z* 16 for O indicates that CO is not a contributor to the peak at *m*/*z* 28. The signal of *m*/*z* 28 (N_2) was also observed in the decomposition of *h*TA, indicating the routes for N_2 formation should include elimination of N–N from the ring.

It is apparent that the peak at *m*/*z* 69 is the molecule of triazole. Table 1 lists two possible structures for triazole, one being 1-*H*-1,2,4-triazole and the other 4-*H*-1,2,4-triazole. Correspondingly, there are two channels for generating triazole from 4-ATAN. The 1-*H*-triazole results from a direct loss of the amino group (NH_2) from 4-ATAN—a process similar to deprotonation, in which NH_2 acts as a "big proton". The second channel, responsible for the formation of 4-*H*-triazole, requires further decomposition of 4-ATA, that is, 4-ATA loses NH_2 and then picks up one H at the site of N_4.

The molecular structure of *m*/*z* 42 is considered to be HCNNH (see Table 1), which is explainable by its daughter ions at *m*/*z* 28 (N_2 or HNCH), 27 (HCN), 29 (NNH), 13 (CH), and 15 (NH). As seen in Fig. 5, the curve of *m*/*z* 42 resembles that of *m*/*z* 69 so well that one might think *m*/*z* 42 is just a fragment of *m*/*z* 69 formed as a result of electron impact. Examination of their intensity ratio (M42/M69) reveals that this is possible. As shown in Fig. 6 the ratio of *m*/*z* 42 to 69 is almost a constant (M42/M69 = 0.9) over the duration of 0.5–3.5 s, suggesting *m*/*z* 42 is likely formed as a fragment of the triazole (*m*/*z* 69) during this period of time.

The NIST standard spectrum of *h*TA also shows a fragment of *m*/*z* 69 at *m*/*z* 42. However a smaller fraction (M42/M69 = 0.63) is reported for an higher electron energy of 70 eV (compared to 22 eV of the current study), which may suggest that fragmentation is not the only source for *m*/*z* 42. The increase in the ratio of M42/M69 after 3.5 s (see Fig. 6) indicates that species of *m*/*z* 42 may also include a contribution due to ring fracture resulting

Table 1
Species from laser-driven decomposition of 1-H-4-amino-1,2,4-triazolium nitrate (electron impact of 22 eV, laser heating at 100 W/cm^2, in 1 atm. helium)

Parent ions		Daughter ions		Probable species	Notes
m/*z*	Possibilities	*m*/*z*	Possibilities		
84	Amino-triazole (ATA)	–	–	Amino-triazole (ATA)	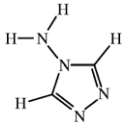
70	[*h*TA + H]	–	–	[*h*TA + H]	Protonation of triazole
69	Triazole	–	–	Triazole	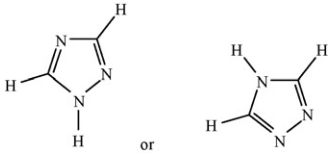
57	[ATA − HCN]	–	–	[ATA − HCN]	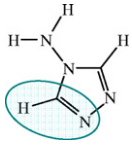
46	NO_2	30[a]	NO	NO_2	Daughter 30 ≫ 14,16
		16	O		
		14	N		
44	N_2O	16	O, NH_2	N_2O	Mainly N_2O (trace H_2CNNH_2 also present in 4-ATA)
	H_2CNNH_2	30	NO	H_2CNNH_2	
		28	H_2CN		
		14	N		
43	$HCNNH_2$	–	–	$HCNNH_2$	Fragment of H_2CNNH_2
42	HCNNH	28	N_2, HNCH	HCNNH	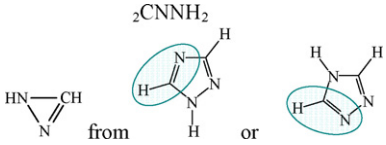
		27	HCN		
		29	NNH		
		13	CH		
		15	NH		
41	CNNH	–	–	CNNH	Fragment of HCNNH (42)
40	CNN	–	–	CNN	Fragment of HCNNH (42)
30	NO	14	N	NO	HNNH also present in 4-ATA
	HNNH	16	O, NH_2	HNNH	
		29	NNH		
		28	N_2		
29	N_2H	–	–	N_2H	Fragment of NNH_2
28	N_2	14	N	N_2	No CO due to the lack of daughter O at *m*/*z* = 16
	CO				
27	HCN	12	C	HCN	
		13	CH		
		14	N		
18	H_2O	–	–	H_2O	
17	NH_3	16	NH_2	NH_3	May also contain fragment of H_2O, but quite small
		15	NH		
16	NH_2	–	–	NH_2	Fragment of NH_3
14	N	–	–	N	Fragment of N_2 and/or NH_3

[a] Daughter ions are listed in descending order of intensity.

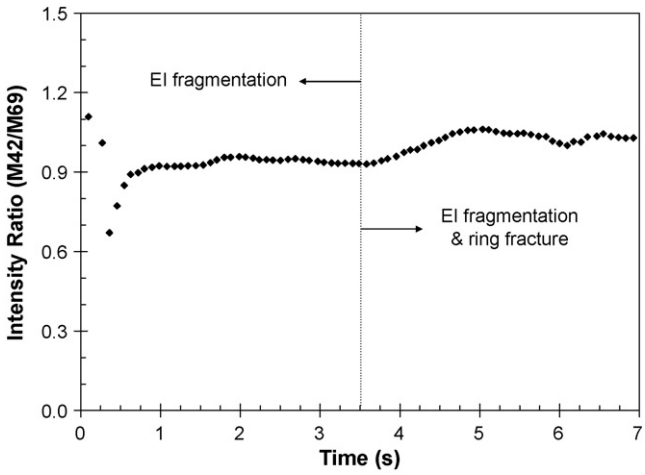

Fig. 6. Examination of possible fragments of triazole and amino-triazole (data taken from Fig. 5).

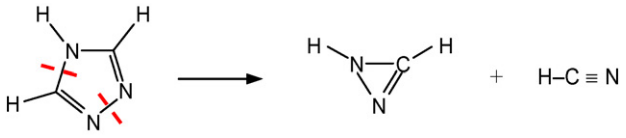

Fig. 7. Decomposition of triazole via cleavage of two single bonds of the ring.

from laser heating, i.e., the triazole (*m*/*z* 69) releases an HCNNH and an HCN through homolysis of two single bonds of the ring, as shown in Fig. 7. The HCNNH could be an open-chain or a three-membered ring, with the latter more stable and thus more likely.

Species for *m*/*z* 30 include NO and HNNH. NO is related to the anion (NO_3^-) while HNNH must originate from the cation. Additional evidence supporting the presence of HNNH is that the signal of *m*/*z* 30 was also observed in the decomposition test with 4-ATA, where NO is not possible because there is no oxygen available. A typical result of 4-ATA is given in Fig. 8, where *m*/*z* 30 is clearly seen. The curve of *m*/*z* 30 follows that of *m*/*z* 84 so well that their intensity ratio is nearly a constant,

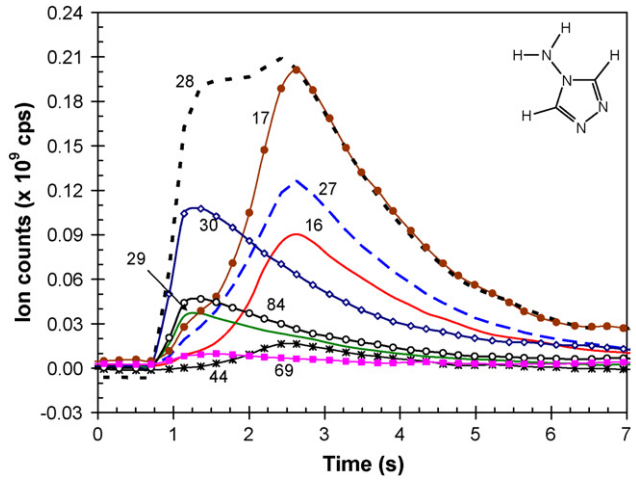

Fig. 8. Decomposition products of 4-amino-1,2,4-triazole at 100 W/cm^2 in helium at 1 atm.

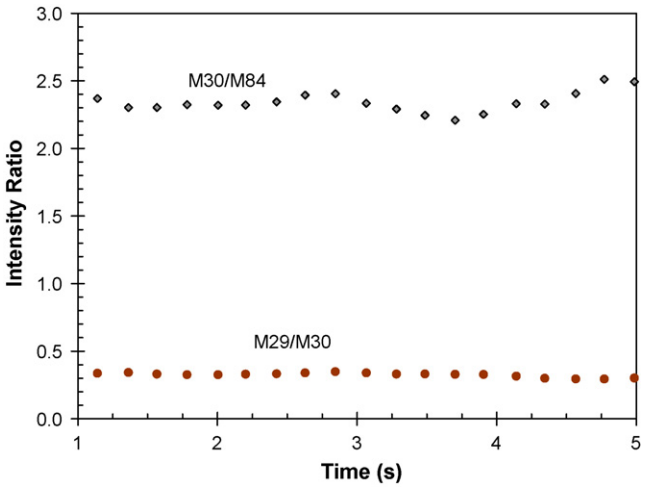

Fig. 9. Examination of possible fragments in decomposition of amino-triazole (data taken from Fig. 8).

as shown in Fig. 9. The amino group in 4-ATA and 4-ATAN must be involved in the formation of HNNH because, without the amino group, the signal of *m*/*z* 30 is not present, as shown in Fig. 10 for the decomposition of *h*TA. It is interesting to note that the peak at *m*/*z* 27 in *h*TA is very small as compared to its larger peak in 4-ATA or 4-ATAN. One possible reason for this difference may be that *m*/*z* 27 is fragmented into smaller species by EI in the case of *h*TA but somehow survived in the cases of 4-ATA and 4-ATAN. More work needs to verify this possibility.

Two species are considered to be possible for the peak at *m*/*z* 44, which are nitrous oxide (N_2O) and $H_2CN\text{-}NH_2$. The daughters at *m*/*z* 16, 30, and 14 are consistent with the calibration result for N_2O. The presence of $H_2CN\text{-}NH_2$ is supported by its daughters *m*/*z* 28 (H_2CN) and *m*/*z* 16 (NH_2). In addition, a peak at *m*/*z* 44 observed in the decomposition of 4-ATA (see Fig. 8) is a sign that $H_2CN\text{-}NH_2$ is also a contributor to *m*/*z* 44 in 4-ATAN decomposition. Since only a small amount of $H_2CN\text{-}NH_2$ is formed in the 4-ATA test, N_2O appears to dominate the signal of *m*/*z* 44 in the decomposition of 4-ATAN.

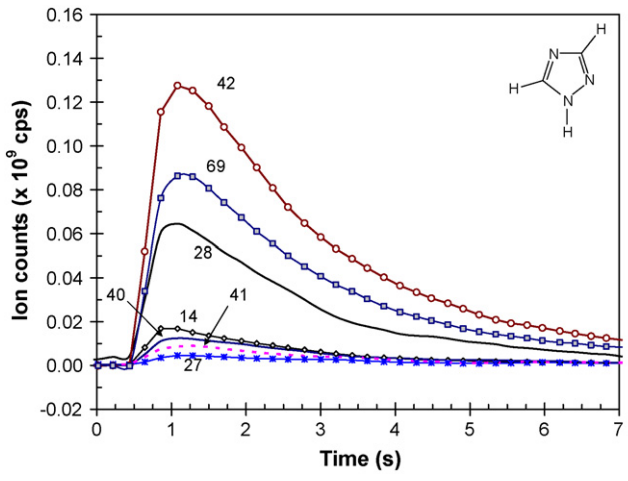

Fig. 10. Decomposition products of 1-*H*-1,2,4-triazole at 100 W/cm^2 in helium at 1 atm. (condensation of gaseous triazole causing sampling orifice blocked).

The nitrogen dioxide (NO_2) represents the peak at *m*/*z* 46, which is confirmed by its daughter ions. It is believed that HCN accounts for *m*/*z* 27, because its daughter ions match well with the standards. Clearly, HCN must be a product as a result of ring opening. Species of *m*/*z* 14 is thought to be the fragment N from N_2 and/or NH_3.

Examination of the daughters for *m*/*z* 17 suggests that the parent species is mainly ammonia (NH_3) and a small fraction (less than 2%) of fragments from water. It appears that EI fragmentation of the ammonia produces ample amidogen radical (NH_2) detected as the peak at *m*/*z* 16. It is noted that both signals at *m*/*z* 17 and *m*/*z* 16 are also detected from 4-ATA (see Fig. 8), but not in tests with hTA (see Fig. 10), indicative of the amino group being the source of ammonia.

Species at *m*/*z* 40 and *m*/*z* 41 are thought to be different EI fragments from HCNNH, the part of *m*/*z* 42 that is formed due to thermal decomposition. The signal of *m*/*z* at 84 is the neutral amino-triazole molecule resulting from deprotonation at site N_1 on the ring.

The nitrogen hydride (N_2H) for *m*/*z* at 29 is likely to be a fragment of HNNH (*m*/*z* 30). This is based on the facts that both signals are also observed in the decomposition of 4-ATA (see Fig. 8), and their intensity ratio is very close to a constant (see Fig. 9). Assignment of *m*/*z* 43 remains tentative; one possibility is $HCNNH_2$ formed as a fragment of $H_2CN\text{-}NH_2$. Another possibility is that the 4-ATA ring opens releasing NNCH and $HCNNH_2$, but this requires breaking one of the double bonds C=N on the ring, which seems less likely.

Protonation of the triazole gives the low intensity signal of *m*/*z* 70. The tiny amount of signal at *m*/*z* 57 results from loss of HCN from the neutral amino-triazole by breaking any two of the three single bonds on the ring, which may be due to either thermal decomposition or electron impact.

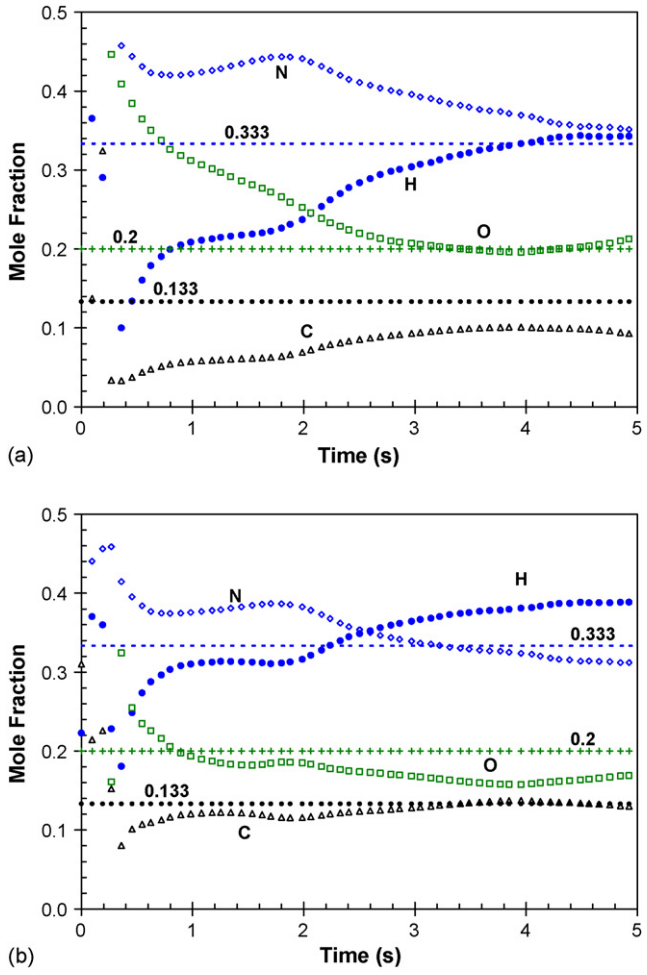

Fig. 11. Element balance for decomposition of 4-ATAN: (a) based on detected gaseous species; (b) re-condensed amino-triazole and triazole were taken into account.

3.4. Quantitative analysis

Sensitivity coefficients were obtained from calibration tests for most of the species that are readily available. Estimation was made for the remaining species based on a close match in their ionization cross sections with that of species for which calibration data are available. Also, analysis of the element balance was performed to help compensate for the loss of triazole (*m*/*z* 69) and amino-triazole (*m*/*z* 84) due to condensation. The intensities (or total ion counts) of species that have significant EI fragments were adjusted based on their standard fragmentation patterns. Some species were omitted due to their very small signal intensities. Since not all the species were taken into account due to difficulty in quantitative differentiation, precise element balance should not be expected.

The analysis for element balance is based on the assumption that, for each sample molecule that decomposes to form gaseous species, the mole fraction of each element in these gaseous species should be equal to its mole fraction in the sample molecule. For a molecule of 4-ATAN ($C_2H_5N_5O_3$), the theoretical mole fractions of its four elements are 0.133 (C), 0.333 (H), 0.333 (N), and 0.2 (O). However, as mentioned above, when conducting the experiments, the sampling orifice was partially blocked in each test. Post-test examination of the orifice surrounding area showed significant deposition of condensed particles. Also, condensation was found to be occurring on the test chamber walls. It is therefore apparent that only part of the gaseous amino-triazole and triazole entered the orifice as gaseous species, while the remaining portions re-condensed and remained outside the mass spectrometer. If the re-condensed species (amino-triazole and triazole) are substantial, as seems likely, elements in the detected gaseous species would not be balanced. Fig. 11a presents the result calculated based on the detected species (the same data set with Fig. 5).

The deviation from the theoretical values is well beyond error tolerance. A major source for the deviation is loss of amino-triazole and triazole due to re-condensation. Since an accurate method is not readily available to determine the fraction of these products that re-condensed, estimation has to be made. Another factor leading to the imbalance of elements is that part of the amino-triazole and/or triazole formed during early decomposition of the sample salt does not vaporize but remains in the condensed phase, while other gaseous products (such as NO, N_2O, NO_2) and lighter species will preferentially leave the sample into the gas phase plume. This may explain the larger

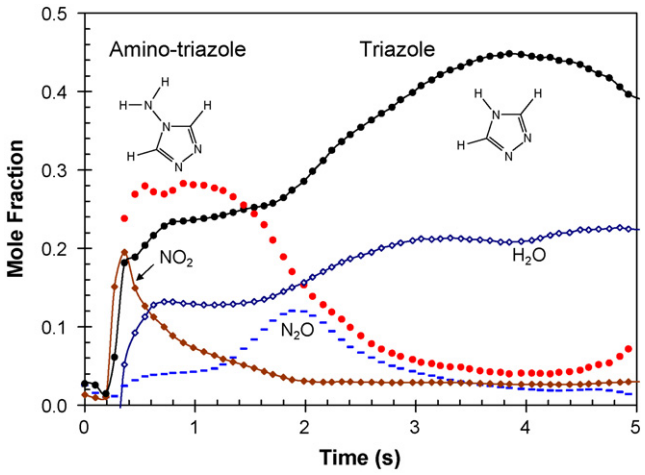

Fig. 12. Quantitative analysis of major products of 4-ATAN decomposition (from the same data set with Fig. 5).

mole fractions of O and N seen in early time of decomposition. Fig. 11b is an adjusted result, which shows substantial improvement in the element balance. Note that the amino-triazole and triazole used in the calculation were both multiplied by a factor of 5. With these adjustments, the quantitative data in mole fraction for some of the major products are provided in Fig. 12. The quantitative data show formation of amino-triazole early in the event and then consumption of itself accompanied by large increase in triazole. This may imply that one route for producing triazole is through decomposition of amino-triazole.

The large amounts of amino-triazole and triazole in the quantitative data show that, with the current test setup/conditions, only a small fraction of the sample may undergo complete decomposition to give final products, for example, HCN. This statement can be easily understood given the fact that the gaseous products (intermediates) are entrained into the helium stream and carried away as soon as they are formed, and thus receive no more laser heating. Therefore, gas phase decomposition should be limited within the current experimental configuration.

3.5. Initiation reactions

From the experimental results, it appears that initiation steps leading to decomposition of 4-ATAN may involve deprotonation at site N_1 followed by proton transfer to form neutral 4-amino-1,2,4-triazole (4-ATA) and nitric acid (NHO_3). This reaction is shown in Fig. 13.

Evidence in support of this scheme is available in the data shown in Fig. 5, where the amino-triazole (*m*/*z* 84) was clearly observed in the early stage of decomposition. However, no

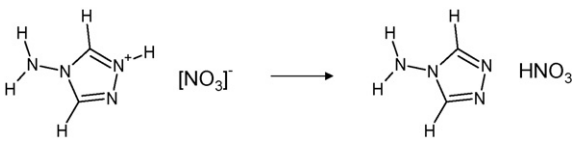

Fig. 13. Possible initiation mechanism: deprotonation at N_1 and proton transfer forming 4-ATA and HNO_3.

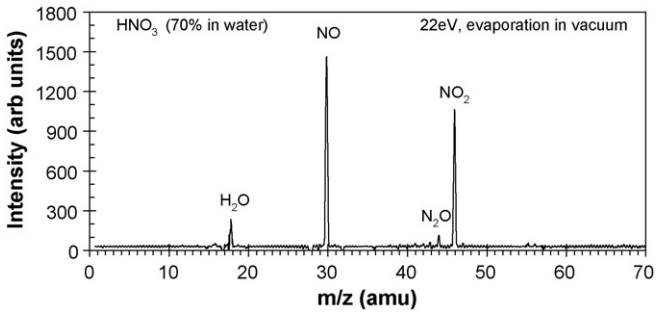

Fig. 14. Mass spectrum of HNO_3 resulting from fragmentation due to electron impact.

detection of nitric acid (HNO_3, *m*/*z* 63) was found using the quadrupole mass spectrometer. In a similar study by our collaborators who used both FTIR and ToF-MS to study the same material (4-ATAN), a considerable amount of nitric acid (*m*/*z* 63) showed up in the FTIR but none in the ToF-MS [50].

It appears that all the nitric acid molecules that enter the mass spectrometers (both TQ-MBMS and ToF-MS) were fragmented due to EI in the ionizer. This was verified by a test with nitric acid (70% solution in water), which is shown in Fig. 14. In this test, laser heating was not applied in order to avoid reactions occurring outside the mass spectrometer, so the obtained spectrum represents the fragments of HNO_3 caused by EI. The spectrum did not show any signal for HNO_3 (even in a trace amount), indicating it was completely fragmented in the EI process. It is important to note that the fragments NO and NO_2 follow a pattern similar to the one seen in the test of 4-ATAN. This indicates that most (if not all) of the signals of NO and NO_2 observed in the test of 4-ATAN are not decomposition products but just fragments of the nitric acid. The absence of NO_2 in the FTIR results [50] confirms the above statement.

Additional evidence in support of proton transfer forming an acid and a neutral amino-triazole is available from test results with 4-ATACl. Fig. 15 provides a typical mass spectrum of 4-ATACl. For comparison, the spectrum of 4-ATAN is also presented in the figure. The presence of hydrochloride at *m*/*z* 36 (with an isotopic ion at *m*/*z* 38) is a sign of proton transfer from the cation to the anion forming acid HCl. The amino-triazole (*m*/*z* 84) is also evident. The absence of H_2O, N_2O, NO_2, and NO (*m*/*z* 30 can only be HNNH in the case of 4-ATACl) is expected because no oxygen is available in 4-ATACl. These results also confirm that these oxygen containing species are products of reactions involving the nitrate (NO_3^-) in 4-ATAN.

The nitric acid formed in 4-ATAN may be consumed in two ways: part of it enters the mass spectrometer as a gas and then undergoes complete fragmentation to form mainly NO and NO_2, while the remaining part remains in the condensed phase to attack products left in the condensed phase and form H_2O and N_2O. Fig. 16 lists a possible route for forming H_2O and N_2O, which is based on an analogy to the low-temperature decomposition of ammonia nitrate (NH_4NO_3) [51]. The high-temperature chemistry of ammonia nitrate [52] suggests a neutral path to N_2O, which involves formation of NO_2. Because NO_2 is thought

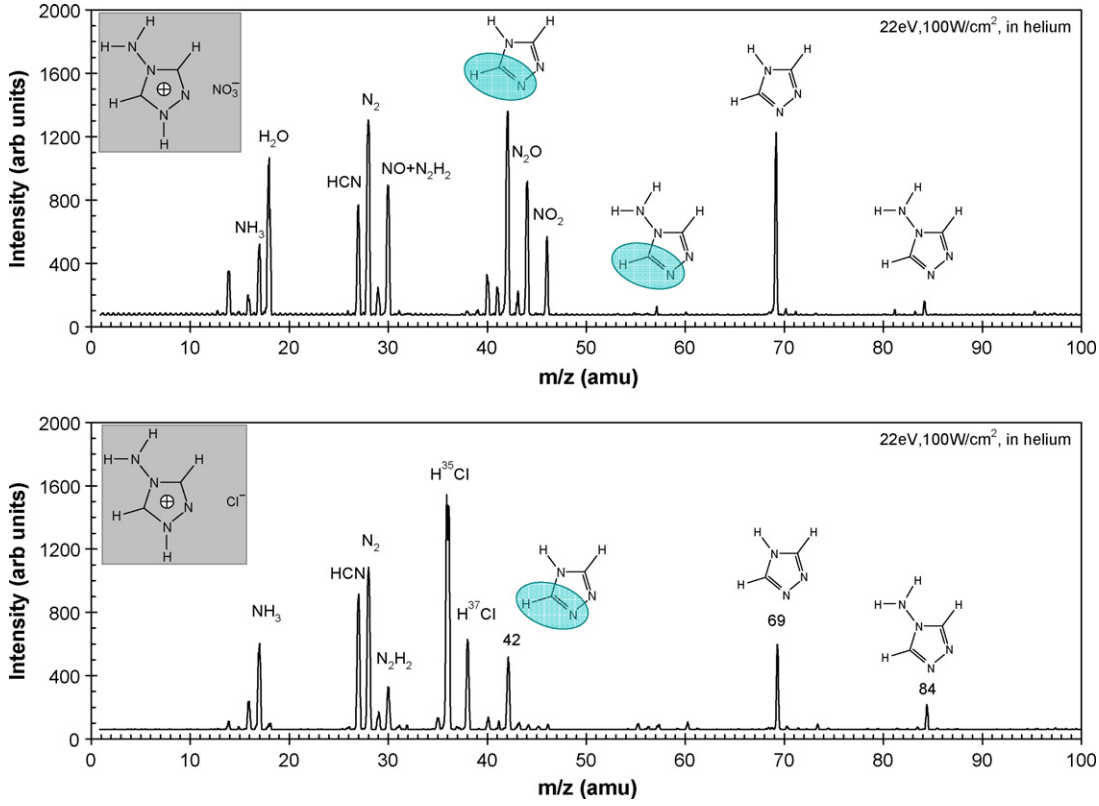

Fig. 15. Mass spectra of 4-ATACl and 4-ATAN (laser heating at 100 W/cm^2, 1 atm. helium).

to be formed as a fragment of nitric acid (not a decomposition product of 4-ATAN), the neutral route is considered less likely.

The process used to synthesize the 4-ATAN salt [52] may also shed light on the statement that deprotonation from the site N_1 is the most likely first step of decompositon, because that is the site for 4-amino-1,2,4-triazole to be quaternized with nitric acid. If 1,2,4-triazole is substituted with amino at N_1, its quaternization occurs at N_4 [53]. It is tempting to think that the initiating reaction of decomposition of the salt tends to reverse the quaternization process via deprotonation, as shown in Fig. 17. Schmidt et al. [54] investigated the 1-*H*-4-amino-1,2,4-triazolium cation through ab initio quantum chemistry calculations and found that deprotonation at N_1 was the most likely initiation reaction based on the energy required for deprotonation.

A remaining issue is whether the amino-group is involved in the initiation reactions. The large signal of triazole (*m*/*z* 69) observed in the data of 4-ATAN (see Fig. 5) seems to suggest so. In addition, Oxley et al. investigated 3,6-substituted tetrazine [55] and its nitrate salt [56], and found decomposition involving the substituent group is possible; in particular, when one of the substituents is amino (NH_2), formation of NH_3 is through protonation of the eliminated NH_2 from the ring.

However, the triazole observed in the data may not be the result of a single initiation reaction, but rather it may be formed in subsequent decomposition reactions. One possibility is displacement of the amino group by a hydrogen radical. The released NH_2 radical would then attack back at a new amino-triazole molecule to form ammonia. This postulated process is shown in Fig. 18.

Another important issue is the formation of N_2. The abundance of N_2 (labeled as 28 in the figures) in the decomposition of

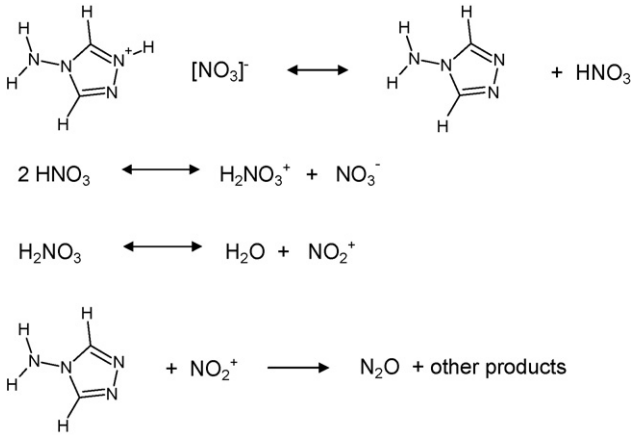

Fig. 16. Formation of oxygen-containing species from radical-driven chain reactions.

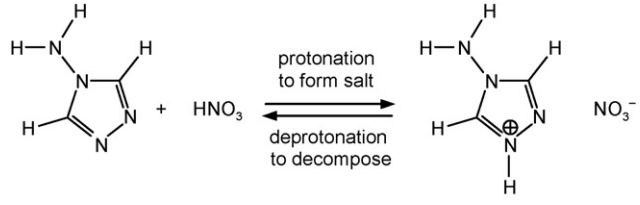

Fig. 17. Formation of salt (4-ATAN) [53] and decomposition starting from proton transfer to form neutral pair.

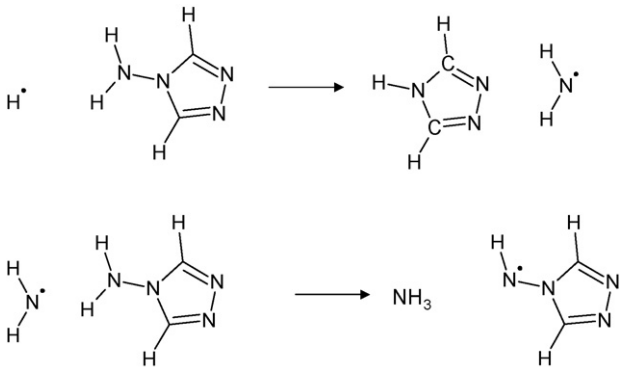

Fig. 18. Formation of triazole and ammonia from neutral amino-triazole.

4-ATA (Fig. 9) and *h*TA (Fig. 10) suggests that the main mechanism of decomposition includes elimination of N_2 from the triazole ring. Moreover, in tests with the chloride salt, N_2 is also evident, which further augments the possibility of N_2 coming from the ring. Therefore, it is likely that most of the N_2 in the data of 4-ATAN is from ring fracture.

For the amino-substituted triazole ring (for 4-ATAN, 4-ATACl and 4-ATA), the possible sources for N_2 formation include N-NH_2 and C=N–N=C, while only the latter for *h*TA. The source of N-NH_2 is more likely, because it requires scission of single bonds. The second source, C=N–N=C, requires cleavage of two double bonds (C=N) to form N_2, and thus is less likely.

4. Summary and conclusion

An experimental work was conducted to study the behavior of an ionic liquid, 1-H-4-amino-1,2,4-triazolium nitrate, during thermal decomposition driven by an infrared laser. A triple quadrupole mass spectrometer with molecular beam sampling was used to obtain gaseous decomposition species of the sample. The principal mass peaks that may contain multiple masses were analyzed through tandem mass techniques. The experiments were conducted at a laser heat flux of 100 W/cm^2 in helium at 1 atmosphere.

The experimental results indicate that the reaction that initiates the decomposition of 1-H-4-amino-1,2,4-triazolium nitrate is proton transfer from site N_1 on the ring to the nitrate forming a neutral pair (nitric acid and amino-triazole). Although nitric acid is not directly observed in the gas-phase products, its ionization fragments, NO_2 and NO, are observed early in the reaction in a ratio that is consistent with calibration results for nitric acid. Elimination of the amino group from the cation ring appears to occur in subsequent decomposition of the neutral amino-triazole, which results in the formation of triazole and ammonia. The data also indicate that formation of N_2 by direct elimination from the ring is the dominant path under the conditions of this study. Based on analogies to the reactions of ammonium nitrate, an ionic route to the formation of N_2O is proposed. Evidence from the current study also shows that the decomposition process involves condensed phase.

Acknowledgments

This work is supported by the U.S. Air Force Office of Scientific Research under Contract No. F49620-03-1-0211, with Dr. Michael Berman serving as the program manager. The authors wish to thank Drs. Hawkins and Drake of Edwards AFB for providing the 4-ATAN material.

References

[1] C.M. Gordon, Appl. Catal. A 222 (2001) 101–117.
[2] M.J. Earle, K.R. Seddon, Pure Appl. Chem. 72 (7) (2000) 1391–1398.
[3] T. Welton, Chem. Rev. 99 (1999) 2071–2083.
[4] J. Dupont, R.F. de Souza, P.A.Z. Suarez, Chem. Rev. 102 (10) (2002) 3667–3692.
[5] J.G. Huddleston, H.D. Willauer, R.P. Swatloski, A.E. Visser, R.D. Rogers, Chem. Commun. (1998) 1765–1766.
[6] H. Olivier-Bourbigou, L. Magna, J. Mol. Catal. A: Chem. 182–183 (2002) 419–437.
[7] J. Brennecke, E.J. Maginn, AICHE J. 47 (11) (2001) 2384–2389.
[8] J.S. Wilkes, J.A. Levisky, R.A. Wilson, C.L. Hussey, Inorg. Chem. 21 (3) (1982) 1263–1264.
[9] J.S. Wilkes, M.J. Zaworotko, J. Chem. Soc. Chem. Commun. (1992) 965–967.
[10] A.A. Fannin, D.A. Floreani, L.A. King, J.S. Landers, B.J. Piersma, D.J. Stech, R.L. Vaughn, J.S. Wilkes, J.L. Williams, J. Phys. Chem. 88 (1984) 2614–2627.
[11] A.S. Larsen, J.D. Holbrey, F.S. Tham, C.A. Reed, J. Am. Chem. Soc. 122 (2000) 7265–7272.
[12] J. Sun, M. Forsyth, D.R. MacFarlane, J. Phys. Chem. B 102 (44) (1998) 8858–8864.
[13] P. Bonhôte, A.-P. Dias, N. Papageorgiou, K. Kalyanasundaram, M. Grätzel, Inorg. Chem. 35 (5) (1996) 1168–1178.
[14] K.-Y. Lee, M.D. Coburn, J. Energ. Mater. 1 (1) (1983) 109–122.
[15] B.C. Beard, J. Sharma, J. Energ. Mater. 7 (3) (1989) 181–198.
[16] B.C. Beard, J. Sharma, J. Energ. Mater. 11 (4–5) (1993) 325–343.
[17] T.R. Botcher, D.J. Beardall, C.A. Wight, L. Fan, T.J. Burkey, J. Phys. Chem. 100 (21) (1996) 8802–8806.
[18] N.L. Garland, H.D. Ladouceur, H.H. Nelson, J. Phys. Chem. A 101 (45) (1997) 8508–8512.
[19] N.J. Harris, K. Lammertsma, J. Am. Chem. Soc. 118 (34) (1996) 8048–8055.
[20] G.T. Long, B.A. Brems, C.A. Wight, J. Phys. Chem. B 106 (15) (2002) 4022–4026.
[21] D.F. McMillen, D.C. Erlich, C. He, C.H. Becker, D.A. Shockey, Combust. Flame 111 (3) (1997) 133–160.
[22] J.A. Menapace, J.E. Marlin, D.R. Bruss, V. Dascher, J. Phys. Chem. 95 (14) (1991) 5509–5517.
[23] C. Meredith, T.P. Russell, R.C. Mowrey, J.R. McDonald, J. Phys. Chem. A 102 (2) (1998) 471–477.
[24] H. Östmark, H. Bergman, G. Åqvist, Thermochim. Acta 213 (1993) 165–175.
[25] J.C. Oxley, J.L. Smith, E. Rogers, X.-X. Dong, J. Phys. Chem. A 101 (19) (1997) 3531–3536.
[26] E.F. Rothgery, D.E. Audette, R.C. Wedlich, D.A. Csejka, Thermochim. Acta 185 (2) (1991) 235–243.
[27] T.S. Sumrall, Propell. Explos. Pyrotech. 24 (2) (1999) 61–64.
[28] W.A. Trzcinski, S. Cudzilo, J. Energ. Mater. 19 (1) (2001) 1–21.
[29] G.K. Williams, S.F. Palopoli, T.B. Brill, Combust. Flame 98 (3) (1994) 197–204.
[30] G.K. Williams, T.B. Brill, J. Phys. Chem. 99 (33) (1995) 12536–12539.
[31] W.-L. Yim, Z.-F. Liu, J. Am. Chem. Soc. 123 (10) (2001) 2243–2250.
[32] T.B. Brill, T.L. Zhang, B.C. Tappan, Combust. Flame 121 (4) (2000) 662–670.
[33] S. Dong, G. Zhang, B. Chen, Y. Ou, H. Jai, Acta Cryst. Sect. C: Cryst. Struct. Commun. 52 (8) (1996) 2057–2058.

[34] A. Finch, P.J. Gardner, A.J. Head, H.S. Majdi, Thermochim. Acta 213 (14) (1993) 17–22.
[35] R. Hu, J. Song, F. Li, B. Kang, Y. Kuong, Z. Mao, Z. Zhou, Z. Hong, Thermochim. Acta 299 (1) (1997) 87–93.
[36] R. Hu, Z. Meng, B. Kang, Thermochim. Acta 275 (2) (1996) 159–172.
[37] K.-Y. Lee, M.M. Stinecipher, Propell. Explos. Pyrotech. 14 (6) (1989) 241–244.
[38] G. Singh, I.P.S. Kapoor, S.P. Felix, J.P. Agrawal, Propell. Explos. Pyrotech. 27 (1) (2002) 16–22.
[39] J. Song, B. Ning, R. Hu, B. Kang, Thermochim. Acta 352–353 (2000) 111–115.
[40] B.C. Tappan, R.W. Beal, T.B. Brill, Thermochim. Acta 388 (1–2) (2002) 227–232.
[41] G. Singh, I.P.S. Kapoor, S.M. Mannan, S.K. Tiwari, J. Energ. Mater. 16 (1) (1998) 31–43.
[42] G. Singh, I.P.S. Kapoor, S.M. Mannan, S.K. Tiwari, J. Energ. Mater. 16 (2–3) (1998) 101–118.
[43] T. Soos, G. Hajos, A. Messmer, J. Org. Chem. 62 (4) (1997) 1136–1138.
[44] H.-H. Licht, H. Ritter, J. Energ. Mater. 12 (4) (1994) 223–235.
[45] Y. Lee, C.-J. Tang, T.A. Litzinger, Meas. Sci. Tech. 9 (9) (1998) 1576–1586.
[46] J.-Q. Li, Ph.D thesis, Dept. of Mechanical and Nuclear Engineering, Pennsylvania State University, 2004.
[47] M. Bobeldijk, W.J. Van der Zande, P.G. Kistemaker, Chem. Phys. 179 (2) (1994) 125–130.
[48] J.-Q. Li, T.A. Litzinger, J. Propul. Power 23 (1) (2007) 166–174.
[49] Y. Dessiaterik, T. Baer, R.E. Miller, J. Phys. Chem. A 110 (2006) 1500–1505.
[50] A. Chodhury, S.T. S Thynell, The Combustion Committee Easter States Conference, 2005.
[51] J.C. Oxley, J.L. Smith, W. Zheng, E. Rogers, M.D. Coburn, J. Phys. Chem. A 101 (1997) 5646–5652.
[52] G. Drake, T. Hawkins, A. Brand, L. Hall, M. Mckay, A. Vij, I. Ismail, Propell. Explos. Pyrotech. 28 (4) (2003) 174–180.
[53] H. Xue, S.W. Arritt, B. Twamley, J.M. Shreeve, Inorg. Chem. 43 (2004) 7972–7977.
[54] M.W. Schmidt, M.S. Gordon, J.A. Boatz, J. Phys. Chem. 109 (2005) 7285–7295.
[55] J.C. Oxley, J.L. Smith, J. Zhang, J. Phys. Chem. A 104 (2000) 6764–6777.
[56] J.C. Oxley, J.L. Smith, H. Chen, Thermochim. Acta 384 (2002) 91–99.